Fluid Phase Equilibria 297 (2010) 149–153

Contents lists available at ScienceDirect

Fluid Phase Equilibria

journal homepage: www.elsevier.com/locate/fluid

High pressure phase equilibria in methane + waxy systems. 2. Methane + waxy ternary mixture

Jérôme Pauly[a], João A.P. Coutinho[b], Jean-Luc Daridon[a,*]

[a] Laboratoire des Fluides Complexes, Université de Pau, BP 1155, 64013 Pau Cedex, France
[b] CICECO, Departemento de Química, Universidade de Aveiro – 3810-193 Aveiro, Portugal

ARTICLE INFO

Article history:
Received 7 April 2010
Received in revised form 14 June 2010
Accepted 15 June 2010
Available online 23 June 2010

Keywords:
Experimental
Vapour–solid–liquid equilibrium
Methane
Wax
Paraffin

ABSTRACT

Liquid–vapour and fluid–solid phase transitions were experimentally determined under pressure on the system methane + a ternary waxy mixture using a full visibility cell. The wax was an approximately equimolar mixture of n-C_{16}, n-C_{17} and n-C_{18}, the composition being chosen to obtain a mixture with an average molecular weight similar to heptadecane. Measurements were performed according to the synthetic method on different mixtures ranging from 0 to 99.5 mol% of methane. The liquid–solid phase transitions were investigated up to 100 MPa and fluid phase boundary was studied in the temperature domain from 293 to 373 K. Measurements performed on this pseudo-binary system were compared to the phase diagram of the binary system methane + heptadecane.

1. Introduction

Crude oils and natural gases are complex fluids containing many components ranging from low to high molecular weight hydrocarbons. Some of the heavy components which are soluble in the fluid under reservoir conditions may precipitate as an organic solid phase when fluid flows out of the reservoir. In particular, heavy paraffins can form waxy deposits when the fluids are cooled down and depressurized from reservoir to ambient conditions even in fluids with low heavy component content [1,2]. Precipitation and subsequent deposition of these waxes in production wells, transportation pipelines, surface facilities, may hinder or eventually totally block the production. Since remediation of the waxy solid deposits is very costly, there is a widespread interest in the development of methods to prevent wax accumulation and fouling. Although wax formation happens through a complex process which involves several physical phenomena, it is of major importance to be able to adequately predict the thermodynamic conditions for paraffin precipitation from reservoir fluids in order to evaluate the potential risks of wax deposition. Most of thermodynamic studies dedicated to wax precipitation were performed with stock tank oils or synthetic liquid mixtures by measuring the wax appearance temperature under atmospheric pressure or by determining the wax content as a function of temperature during a cooling process. However, in gas-rich fluids such as gas condensates, the depressurization plays a very important role on the development of conditions for wax precipitation and deposition. The consequence of pressure drop on wax formation results from the depressurization itself [3–5] but also from the change of composition caused by the related retrograde condensation [6,7] as well as by the Joule–Thomson cooling effect [8,9]. In order to understand the phase behaviour of gas condensates containing high molecular weight hydrocarbons, Flöter et al. [10–15] and Machado and de Loos [16] studied extensively the phase diagrams of asymmetric binary systems composed of methane and a heavy hydrocarbon constituent. Moreover, Machado and de Loos [17] studied solid precipitation in the model system made of methane + two paraffins. However, in real systems, heavy fraction contains long distributions of heavy components and wax formation involves the precipitation of several paraffins in the same solid solution [18]. It was already noticed by studying the phase behaviour of different type of paraffin distribution in liquid solvent [19–21] that the shape of the distribution has a strong influence on wax appearance condition.

The influence of the size of distribution and its interaction with light ends and in particular methane is not fully identified and need to be better understood in order to extrapolate to live oils or condensate gases the measurements performed on stock tank oils. With this goal in mind, we have begun, as part of project on characterisation of wax precipitation, a programme of phase behaviour measurements on systems made up of a gas (or a mixture of gases) and different heavy waxy fraction starting from the simplest (pure component) to the more complex (heavy fraction coming from con-

* Corresponding author.
E-mail address: jean-luc.daridon@univ-pau.fr (J.-L. Daridon).

0378-3812/$ – see front matter © 2010 Elsevier B.V. All rights reserved.
doi:10.1016/j.fluid.2010.06.009

densation of real condensate gas). In this paper, which follows on a first work on the binary mixture methane + n-heptadecane [7], fluid–solid and fluid phase equilibria measurements were performed of a pseudo-binary system made up of a methane + a mixture of three paraffins ranging from n-C_{16} to n-C_{18}. In order to compare the phase diagram of the pseudo-binary system to the binary methane + n-heptadecane, the composition of the ternary waxy mixture was defined in a way to have an average molecular weight equivalent to those of pure heptadecane. Measurements were performed by the synthetic technique on different mixtures with compositions of methane ranging from 0 to 99%. The fluid phase equilibrium conditions were measured from the wax appearance temperature to 373 K whereas the fluid–solid boundary was determined from atmospheric pressure up to 90 MPa.

2. Experimental

Fluid–fluid and fluid–solid phase transitions were measured by a synthetic method which avoids sampling and analysing of the phases [22]. The apparatus, which has been described in detail in a previous paper [7], is composed of a high-pressure cell which consists in a stainless steel cylinder closed at one end by a sapphire window allowing for a full visibility of the studied fluid. The other end is closed with a moving piston which is able to produce a pressure up to 100 MPa inside the cell. A video acquisition system, made up of an endoscope plus a video camera, is placed right in front of the sapphire window and connected to a screen for observation of the phase transitions occurring inside the cell. The temperature is thermo-regulated by circulating a heat-carrier fluid through flow lines managed in the cell. The heat-carrier fluid is regulated itself with temperature stability of 0.01 K by means of a thermostat bath circulator (Haake). The temperature is measured with a calibrated platinum resistance inserted inside the cell and connected to a high-precision thermometer (AOIP). The pressure is measured by a piezoresistive silicon pressure transducer (Kulite) placed inside the cell in order to reduce the dead volume. As this pressure transducer is subject to the same temperature changes than the cell, it needs to be calibrated as a function of temperature. This calibration was done with an accuracy better than 0.02% in the full temperature and pressure range using a dead weight gauge (Budenberg brand).

The gas + wax systems were directly prepared in the measuring cell at the desired compositions. The waxy ternary mixture was previously prepared by weighing in an auxiliary tank and then introduced in a liquid state in the measurement cell. The exact mass of wax introduced was determined by weighing the auxiliary tank with a precision balance (Ohaus) with an accuracy of 0.1 mg. Finally, the gas was added under pressure from an aluminium reservoir tank (Gerzat) able to resist to 25 MPa fixed in the plate of high weigh/high precision balance with an accuracy of 1 mg (Sartorius) and connected to the measuring cell by means of a flexible high pressure capillary. The amount of gas transferred to the cell was also determined by weighing the gas tank during the filling.

Applying the synthetic method, the phase boundary of a mixture of known composition is established by observing visually the disappearance from a heterogeneous state of one of the phases by changing either the temperature or the pressure conditions. For fluid phase transitions, measurements were carried out by observing the pressure of the disappearance of the vapour or liquid phase during an isothermal process whereas fluid–solid phase transitions were mostly determined by measuring the solid disappearance temperature at a fixed pressure. During both measurements, *P–T* conditions are changed stepwise and the mixture is continuously mixed by a magnetic stirrer placed inside the cell in order to keep the system close to equilibrium during all the experiment. Using this method, wax disappearance temperatures are reproducible to within ±0.1 K whereas reproducibility of bubble or dew pressure is within ±0.05 MPa.

The methane used in this study was supplied by Messer with a guarantee of 99.99% purity. The paraffins were used as supplied by Fluka with a purity better than 99%.

Table 1
Waxy fraction behaviour.

mol% of n-C_{16}	mol% of n-C_{17}	mol% of n-C_{18}	Mw (g mol^{-1})	α	T^m
35.31	33.27	31.42	239.93	0.94	293.95

3. Results and discussion

The wax used on this work, composed of n-C_{16}, n-C_{17} and n-C_{18}, was prepared with the same mass of each paraffin in order to obtain a wax with an average molecular weight close to that of the pure heptadecane. This choice leads to a molar fraction composition with a regular decrease according to recurrence relationship:

$$Xc_{n+1} = \alpha Xc_n$$

with a coefficient α equal to 0.94. The exact composition of the wax is presented in Table 1 along with the average molecular weight of this mixture.

The phase behaviour of the pseudo-binary system methane + wax was studied using isoplethic measurements performed on several mixtures of well-known composition in methane ranging from 0 to 99.5 mol%. The solid–liquid phase transitions were determined for the pure heavy fraction up to 80 MPa by using a high pressure microscopic technique described elsewhere [23]. The results are summarized in Table 2 and plotted in Fig. 1 along with the melting line of the pure heptadecane. As can be noticed in this figure, the general shape of the boundary curves between the monophasic liquid region and the two-phases region is very close to those of pure heptadecane. A shift in temperature of only 1.4 K is observed at atmospheric pressure due to the lower melting points of mixed crystals when compared with pure compounds. Moreover, the average slope (0.210 K MPa^{-1}) between atmospheric and 80 MPa is just a little lower than those of pure heptadecane (0.215 K MPa^{-1}). This difference indicates the existence of a small excess volume in liquid and solid solutions that have to be taken into account when the modelling of phase equilibria is attempted [24–26].

Both fluid–fluid and fluid–solid transitions were determined for all other mixtures. The results are listed in Table 2 along with indication of the nature of the phase boundary. Bubble points were observed in mixtures containing up to 90% whereas only dew points

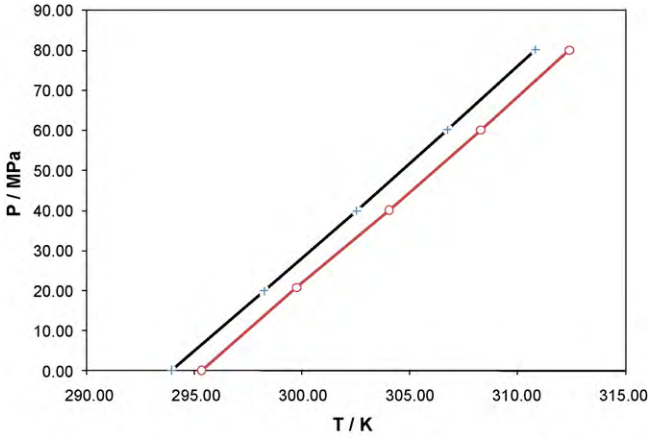

Fig. 1. Liquid–solid phase transition temperatures of the waxy fraction (+) and the pure heptadecane [7] (○) as a function of pressure.

Table 2
Fluid–fluid and fluid–solid phase transitions at a given overall composition (in mol%) of the system methane + waxy fraction.

T (K)	P (MPa)		T (K)	P (MPa)		T (K)	P (MPa)	
0% of CH_4								
293.95	0.1	L + S → L	298.25	19.94	L + S → L	302.55	39.96	L + S → L
306.75	60.20	L + S → L	310.85	80.26	L + S → L			L + S → L
19.90% of CH_4								
292.35	4.24	L + V → L	304.55	4.49	L + V → L	312.75	4.66	L + V → L
323.05	4.85	L + V → L	332.95	5.03	L + V → L	344.65	5.21	L + V → L
353.65	5.31	L + V → L	362.25	5.40	L + V → L	290.75	4.22	Crossover
291.95	10.04	L + S → L	296.15	29.57	L + S → L	300.25	49.53	L + S → L
304.35	69.49	L + S → L	308.45	89.32	L + S → L			
41.77% of CH_4								
291.15	11.37	L + V → L	293.65	11.51	L + V → L	298.45	11.70	L + V → L
304.15	12.01	L + V → L	313.45	12.32	L + V → L	324.45	12.67	L + V → L
333.65	12.97	L + V → L	342.35	13.27	L + V → L	352.15	13.62	L + V → L
361.85	13.80	L + V → L	288.75	7.50	L + V + S → L + V	287.05	11.14	Crossover
288.65	20.01	L + S → L	292.55	40.00	L + S → L	296.25	59.94	L + S → L
299.85	79.60	L + S → L	301.65	89.58	L + S → L			
59.97% of CH_4								
288.15	24.32	L + V → L	293.55	24.47	L + V → L	295.35	24.54	L + V → L
303.35	24.86	L + V → L	313.35	25.06	L + V → L	322.65	25.27	L + V → L
333.15	25.63	L + V → L	342.75	25.79	L + V → L	353.45	25.96	L + V → L
362.85	26.10	L + V → L	284.15	24.20	Crossover	285.55	32.48	L + S → L
286.85	40.31	L + S → L	290.25	60.09	L + S → L	294.95	89.52	L + S → L
78.10% of CH_4								
282.95	54.23	L + V → L	285.15	53.71	L + V → L	288.35	53.25	L + V → L
292.55	52.62	L + V → L	302.45	51.44	L + V → L	313.05	50.44	L + V → L
322.15	49.80	L + V → L	333.15	49.04	L + V → L	343.25	48.32	L + V → L
353.35	47.69	L + V → L	363.45	47.22	L + V → L	285.25	18.59	L + V + S → L + V
283.55	30.17	L + V + S → L + V	282.95	40.19	L + V + S → L + V	282.65	54.55	Crossover
283.45	62.36	L + S → L	284.45	70.37	L + S → L	285.65	80.28	L + S → L
286.95	90.57	L + S → L						
89.48% of CH_4								
282.90	77.69	L + V → L	285.65	76.66	L + V → L	294.25	73.61	L + V → L
300.65	71.64	L + V → L	313.45	68.85	L + V → L	323.15	66.80	L + V → L
333.05	64.98	L + V → L	343.05	63.39	L + V → L	353.35	61.91	L + V → L
283.25	35.09	L + V + S → L + V	282.75	50.22	L + V + S → L + V	282.80	65.00	L + V + S → L + V
282.90	77.69	Crossover	283.45	85.63	L + S → L	283.95	90.71	L + S → L
92.95% of CH_4								
284.95	79.10	L + V → L	288.15	77.74	L + V → L	293.15	75.98	L + V → L
297.85	74.68	L + V → L	303.95	72.88	L + V → L	313.65	70.38	L + V → L
323.25	68.43	L + V → L	333.15	66.41	L + V → L	343.25	64.61	L + V → L
353.15	63.14	L + V → L	362.65	61.71	L + V → L	282.85	47.70	L + V + S → L + V
282.95	65.70	L + V + S → L + V	283.25	80.19	Crossover			
96.00% of CH_4								
283.25	78.50	L + V → V	285.05	78.04	L + V → V	288.15	76.94	L + V → V
293.05	75.12	L + V → V	297.55	73.56	L + V → V	303.55	72.16	L + V → V
313.35	69.63	L + V → V	322.65	67.77	L + V → V	332.95	65.68	L + V → V
342.85	63.92	L + V → V	352.45	62.35	L + V → V	362.95	60.89	L + V → V
283.05	40.34	L + V + S → L + V	282.95	50.43	L + V + S → L + V	283.00	65.60	L + V + S → L + V
283.25	78.50	Crossover	283.35	85.65	V + S → V	283.55	95.94	V + S → V
99.00% of CH_4								
283.45	60.45	L + V → V	289.15	59.66	L + V → V	293.85	58.60	L + V → V
303.15	56.88	L + V → V	312.15	55.19	L + V → V	322.75	53.24	L + V → V
332.55	51.78	L + V → V	343.05	50.26	L + V → V	352.95	49.05	L + V → V
362.25	47.90	L + V → V	283.55	29.91	L + V + S → L + V	283.15	40.49	L + V + S → L + V
283.15	47.88	L + V + S → L + V	283.35	56.24	L + V + S → L + V	283.45	60.45	Crossover
282.35	65.72	V + S → V	281.65	70.61	V + S → V	281.15	75.72	V + S → V
280.73	81.39	V + S → V						
99.50% of CH_4								
283.50	47.50	L + V → V	286.75	47.12	L + V → V	293.15	46.57	L + V → V
302.55	46.11	L + V → V	313.05	45.10	L + V → V	323.75	44.08	L + V → V
332.95	43.15	L + V → V	342.35	42.24	L + V → V	352.55	41.32	L + V → V
283.36	36.51	L + V + S → L + V	283.35	42.88	L + V + S → L + V	283.50	47.50	Crossover
282.05	54.10	V + S → V	281.29	57.72	V + S → V	279.55	69.86	V + S → V
278.65	92.68	V + S → V						

were found for mixtures with a methane content higher than 96%. Phase transitions close to critical conditions were observed in the temperature range investigated for the mixture containing 93% of methane. Since the system is not a real binary system, the three phase S + L + V equilibrium is not monovariant. It corresponds to a narrow area in the P–T projection limited by different kind of boundary according to the nature of disappearance phase. However, only the phase boundary between the three phases L + V + S

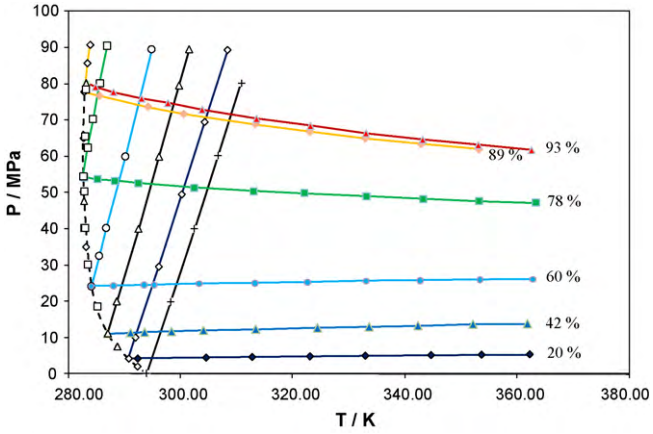

Fig. 2. *P–T* phase diagram of the system methane + waxy fraction for overall compositions (in mol% of CH_4) corresponding to bubble points.

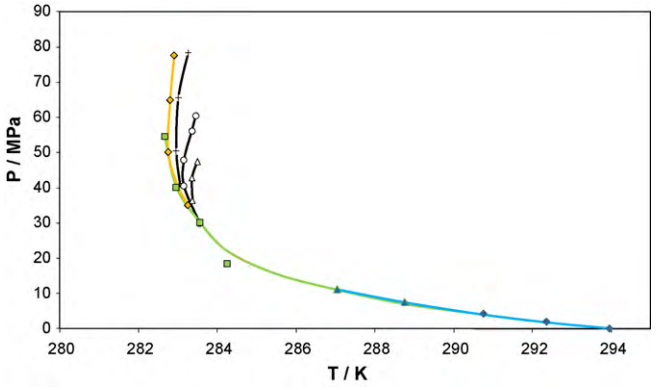

Fig. 4. *P–T* projection of the phase boundary between the liquid–vapour and the liquid–vapour–solid phase region for various overall compositions of the system methane + waxy fraction: (♦) 20% of CH4, (▲) 42% of CH4, (■) 78% of CH4, (◆) 89% of CH4, (+) 96% of CH4, (○) 99% of CH4, (△) 99.5% of CH4.

and the two phases L + V equilibrium regions were determined experimentally by measuring the disappearance conditions of the last solid particle. The end of this phase boundary (called crossover point in Table 2) was indirectly deduced by recording the intersection of the bubble (or dew) curve with fluid–solid transition line. The combined data allowed the plotting of the isopleth *P–T* diagrams. These diagrams are shown in Fig. 2 for mixtures exhibiting bubble points and in Fig. 3 for mixtures leading to dew points. The curves, represented in dashed lines, corresponding to the phase boundary between the three phases L + V + S and the two phases L + V regions of each mixture are very similar for the various mixtures. However, as can be observed in Fig. 4 which focuses on this phase transition, the curves do not overlap as in a binary system. In particular, for high gas content mixtures, these isopleth curves break away towards high temperatures when the pressure increases. Consequently, the *P–T* projection (Fig. 5) of the crossover points between fluid–fluid and fluid–solid transition lines presents two characteristic points: one corresponding to a maximum in pressure and the other to a minimum in temperature. The existence of the minimum in temperature is a common behaviour in such asymmetric mixtures with methane and a heavy hydrocarbon. It was previously observed on the three phase S + L + V curve for most of the methane–heavy alkane binary mixtures [10,22,27,28] and in particular for the binary system C_1–n-C_{17} [7]. The occurrence of a minimum in temperature along the L–V–S curve is not observed for all asymmetric mixture. It implies that the initial slope of the L–V–S in the *P–T* projection is negative and positive beyond the minimum and therefore the volume of transformation change of sign from positive to negative [29,30]. It leads to a retrograde crystallisation phenomena during an isothermal pressure decrease. Actually, for methane compositions higher than those corresponding to this minimum, an isotherm crosses twice the phase boundary between L–V and L–V–S. Thus, waxy solid phase can appear under decompression for isotherms ranging from this minimum to the solid appearance temperature at atmospheric pressure. On the opposite, the presence of a maximum in pressure is not observed on the S + L + V curve of binary systems for which three phase S + L + V equilibrium is monovariant. This maximum shows that the waxy fraction does not crystallise as a single pseudo-component but instead it really crystallises like a mixture. In such waxy mixtures, just below the wax appearance temperature heaviest paraffins crystallise preferentially [31,32] whereas the lightest paraffins remain in the liquid phase. Consequently in the vicinity of the solid appearance conditions, the precipitated solid solutions have a higher content of high molecular weight paraffins than the overall composition. The same behaviour occurs for the liquid–vapour equilibrium where the paraffins do not have the same composition in the liquid and vapour phases. As the system is not monovariant in the three phase equilibrium conditions, the composition of the wax part in each phase varies with the overall composition. In particular when the methane content is higher than the critical composition the liquid phase becomes richer in the heaviest paraffins and the wax appearance temperature increases.

The comparison, presented in Fig. 5, of the projection of the crossover points between fluid–fluid and fluid–solid of the pseudo-

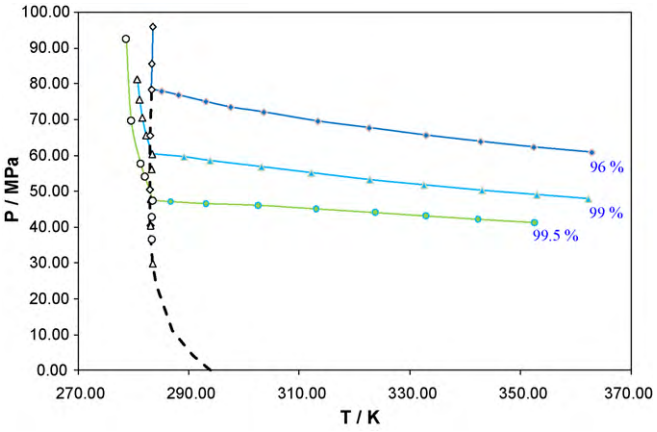

Fig. 3. *P–T* phase diagram of the system methane + waxy fraction for overall compositions (in mol% of CH_4) corresponding to dew points.

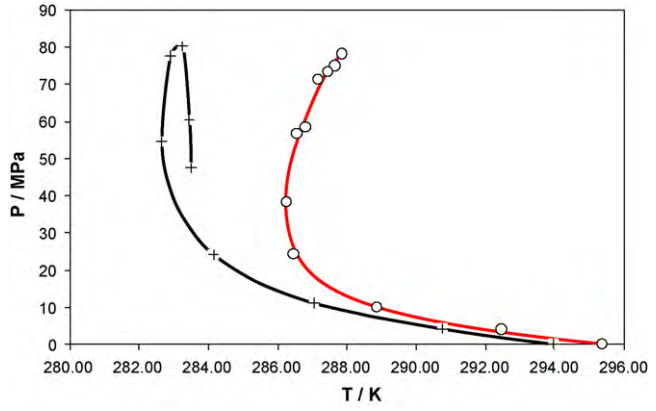

Fig. 5. Comparison of the the three phase L + V + S phase equilibrium curve of the binary system C_1–C_{17} (○) [7] with the *P–T* projection of the *crossover point* of the pseudo-binary system (+).

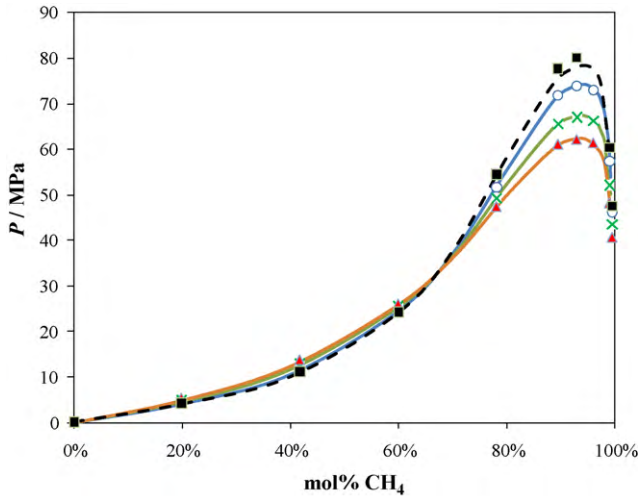

Fig. 6. *P–x* Phase diagram. Point: Pseudo-binary system, line: binary C_1–C_{17} [7]. (■) Crossover points, (○) T = 300 K; (X) T = 330 K; (▲) T = 360 K.

binary system with the L–V–S three phase equilibrium curve of binary system C_1–n-C_{17} brings to light a global pressure effect a little more pronounced for the pseudo-binary mixture than for the C_1–n-C_{17} binary system. The temperature drop observed between the melting temperature at atmospheric pressure and the minimum L–V–S equilibrium curve is about 9 K for the binary C_1–n-C_{17} whereas it reaches 11 K for the pseudo-binary system although the methane content of the liquid phase at wax appearance condition is exactly the same (Fig. 6) as those of real binary system. Consequently, this difference results from the composition of paraffins in the waxy fraction and their distribution between the different phases.

As in the binary system C_1–C_{17}, it can be observed in Fig. 2 that the crystallisation lines are approximately parallel to the melting line of heavy fraction for methane contents inferior to 80 mol%. It appears thus that in this range of composition the presence of methane does not affect the molar partial volume of each paraffin in the mixture. The opposite was found at high methane concentrations, corresponding to gas state. Here, the huge influence of methane leads to negative slopes of crystallisation line as shown in Fig. 3. This induces a cusp shape at the intersection of the wax appearance line with the dew point curve on theses mixture as presented in Fig. 7. This singularity which was also observed [2] in reservoir fluids such as gas condensates, is more strongly marked as the methane content is important.

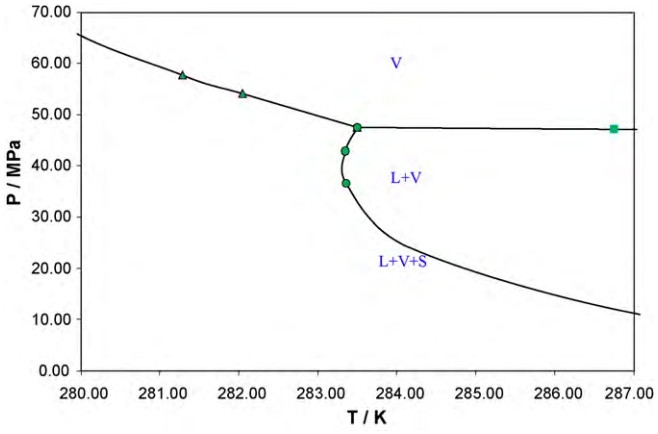

Fig. 7. Cusp point for the mixture with 99.5% of CH_4.

From interpolation of the measurements it was possible to plot the vapour–liquid *P–x* phase diagrams for various isotherms. These phase diagrams are displayed along with that of binary system C_1–C_{17} in Fig. 6 for 3 temperatures above 300 K. This figure reveals a perfect agreement between the two sets of data. Consequently, the waxy part can be treated as a single pseudo-component with a molar mass equal to the average molar mass of the heavy fraction when considering only fluid–fluid phase transitions.

In conclusion, the influence of methane on a waxy heavy fraction made up of n-C_{16} + n-C_{17} + n-C_{18} in a ratio designed so as to get the same molar mass as heptadecane is very similar to those of CH_4 on pure heptadecane. Differences are only observed on the fluid–solid phase transitions for the systems with high methane content despite the fact heavy component are very close. For these more complex systems a sharp cusp point is observed on the crystallisation curve in the neighbourhood of the dew point as shown in Fig. 7. Fluid phase equilibria of both pseudo-binary and binary systems are seen identical. The reason for this observation is that the components of the heavy part belong from the same family and that the distribution is continuous. Therefore the heavy fraction really acts like a pseudo-component and the system can be assimilated to a binary one. If the heavy fraction is made up of components that differ more in nature or in molecular weight a marked influence is observed [32,33].

References

[1] P. Ungerer, B. Faissat, C. Leibovici, H. Zhou, E. Behar, G. Moracchini, J.P. Courcy, Fluid Phase Equilib. 111 (1995) 287–331.
[2] J.L. Daridon, J. Pauly, J.A.P. Coutinho, F. Montel, Energy Fuels 15 (2001) 730–735.
[3] V. Ruffier Meray, J.L. Volle, C.J.P. Schranz, P. Le Marechal, E. Behar, SPE 26549 (1993) 369–373.
[4] T.S. Brown, V.G. Niesen, D.D. Erickson, SPE 28505 (1994) 415–430.
[5] J.L. Daridon, P. Xans, F. Montel, Fluid Phase Equilib. 117 (1996) 241–248.
[6] M.R. Jensen, P. Ungerer, B. de Weert, E. Behar, Fluid Phase Equilib. 208 (2003) 247–260.
[7] J. Pauly, J.A.P. Coutinho, J.L. Daridon, Fluid Phase Equilib. 255 (2007) 193–199.
[8] D.V. Nichita, D. Bessieres, J.L. Daridon, Energy Fuel 22 (2008) 4012–4018.
[9] D.V. Nichita, J. Pauly, J.L. Daridon, Int. J. Thermophys. 30 (2009) 1130–1143.
[10] E. Flöter, Th.W. de Loos, J. de Swaan Arons, Int. J. Thermophys. 16 (1995) 185–194.
[11] E. Flöter, Th.W. de Loos, J. de Swaan Arons, Fluid Phase Equilib. 117 (1996) 153–159.
[12] E. Flöter, Th.W. de Loos, J. de Swaan Arons, Fluid Phase Equilib. 127 (1997) 129–146.
[13] E. Flöter, C. Brumm, Th.W. de Loos, J. de Swaan Arons, J. Chem. Eng. Data 42 (1997) 64–68.
[14] E. Flöter, P. van der Pijl, Th.W. de Loos, J. de Swaan Arons, Fluid Phase Equilib. 134 (1997) 1–19.
[15] E. Flöter, B. Hollanders, Th.W. de Loos, J. de Swaan Arons, Fluid Phase Equilib. 143 (1998) 185–203.
[16] J.J.B. Machado, Th.W. de Loos, Fluid Phase Equilib. 222–223 (2004) 261–267.
[17] J.J.B. Machado, Th.W. de Loos, Fluid Phase Equilib. 226 (2004) 83–90.
[18] J.A.P. Coutinho, J.L. Daridon, Petroleum Sci. Technol. 23 (2005) 1113–1128.
[19] V. Chevallier, M. Bouroukba, D. Petitjean, M. Dirand, J. Pauly, J.L. Daridon, V. Ruffier-Meray, Fuel 79 (2000) 1743–1750.
[20] J. Pauly, J.L. Daridon, J.M. Sansot, J.A.P. Coutinho, Fuel 82 (2003) 595–601.
[21] J. Pauly, J.L. Daridon, J.A.P. Coutinho, Fluid Phase Equilib. 187–188 (2001) 71–82.
[22] H.J. van der Kooi, E. Flöter, Th.W. de Loos, J. Chem. Thermodyn. 27 (1995) 847–861.
[23] J.L. Daridon, J. Pauly, M. Milhet, Phys. Chem. Chem. Phys. 4 (2002) 4458–4461.
[24] J. Pauly, J.L. Daridon, J.A.P. Coutinho, N. Lindeloff, S.I. Andersen, Fluid Phase Equilib. 167 (2000) 145–159.
[25] J.M. Sansot, J. Pauly, J.L. Daridon, J.A.P. Coutinho, AIChE J. 51 (2005) 2089–2097.
[26] U.K. Deiters, S.L. Randzio, Fluid Phase Equilib. 260 (2007) 87–97.
[27] M. Glaser, C.J. Peters, H.J. Van Der Kooi, J. Chem. Thermodyn. 17 (1985) 803–815.
[28] S.L. Randzio, Ch. Stachowiak, J.P.E. Grolier, J. Chem. Thermodyn. 35 (2003) 639–648.
[29] Th.W. de Loos, J. Supercrit. Fluids 39 (2006) 154–159.
[30] J. Gregorowicz, Fluid Phase Equilib. 240 (2006) 29–39.
[31] J.L. Daridon, C. Dauphin, Meas. Sci. Technol. 10 (1999) 1309–1314.
[32] Th.W. de Loos, W. Poot, R.N. Lichtenthaler, Ber. Bunsenges. Phys. Chem. 88 (1984) 855–859.
[33] Th.W. de Loos, W. Poot, R. Perbal, R.N. Lichtenthaler, Ber. Bunsenges. Phys. Chem. 89 (1985) 846–850.